Ni-doped ZnO nanorods/Ti_3C_2 MXene composites and their photocatalytic performance

W. J. Zeng[a], Y. Zhuang[b,*], M. Khan[a], X. T. Ning[c], L. F. Shan[c], B. Zeng[a]
[a]*College of Mechanical Engineering, Hunan University of Arts and Science, Changde 415000, P. R. China*
[b]*Mechanical-Electrical Engineering Faculty, Hunan Institute of Traffic Engineering, Hengyang 421001, P. R. China*
[c]*School of Materials and Environmental Engineering, Hunan University of Humanities, science and Technology, Loudi, 417000, P. R. China*

Herein, composites based on Ni-doped ZnO nanorods and Ti_3C_2 MXene structure (Ni-ZnO NR/Ti_3C_2) were produced via a simple hydrothermal method for photocatalytic applications. Special attention was paid to their structural and optical properties. The composite exhibited a photocatalytic effectiveness of 88.2% in degrading methyl orange (MO) within a duration of 75 minutes when exposed to a xenon lamp. The enhancement of the catalytic activity was due to the one-dimensional ZnO nanostructure, the Ni doping, and the Schottky heterojunction is formed by the interface within ZnO and Ti_3C_2. Therefore, this work provides an effective strategy to fabricate metal oxide/MXene photocatalysts.

(Received April 14, 2024; Accepted July 22, 2024)

Keywords: Ti_3C_2 MXene, Schottky heterojunction, Photocatalytic performance

1. Introduction

Photocatalysis is a perspective technology in the fields relying on water treatment [1]. Thanks to its stable chemical properties, low toxicity and high photocatalytic activity, zinc oxide (ZnO) has garnered significant interest from scientists [2]. Among the different nanostructures, the one-dimensional ZnO nanostructure possesses the high area of surface to volume fractions and the efficient paths for charge carrier transfer are notable features, which can result in high photocatalytic activity [3]. However, a fast carrier recombination reduces the efficiency of photocatalysts.

In recent years, two-dimensional MXenes with fascinating electronic and optical properties have aroused increasing interest [4]. In particular, Ti_3C_2 MXene combined with ZnO can generate a Schottky junction, and the built-in electric fields between them can improve the hole-electron separation [5]. For examples, Tian [6] reported a ZnO/Ti_3C_2 MXene composite with the Schottky junction, whereby the photocatalytic degradation performance of 94.84% could be reached. Le [7] prepared TiO_2/Ti_3C_2 nanoflowers which exhibited extraordinary photocatalytic efficiency toward Rhodamine.

One the other hand, ZnO still suffers from low visible-light absorption because of its wide band gap [8]. The addition of transition metallic elements (Fe, Co, Ni, and Mn) has been discovered as an efficient method to decrease the energy gap of ZnO. [9,10]. Among the various transition metals, Ni has the same valence state and ionic radius with Zn [11]. This enables the latter to be easily substituted in the ZnO lattice, forming a new doping level between the valence band and the conduction band. For example, Aravind et al., [12] produced Ni-doped ZnO via hydrothermal method, which effectively removed Malachite Green dye from aqueous media. Khan et al., [13] prepared Ni-doped ZnO nanocomposites with the photocatalytic activity up to 83.39%.

* Corresponding author: 21467855@qq.com
https://doi.org/10.15251/DJNB.2024.193.1107

Herein, Nanorods of ZnO doped with Ni wrapped with Ti_3C_2 MXene were produced using hydrothermal heating. The composites were subjected to MO degradation studies in order to assess their photocatalytic efficacy, and a corresponding photocatalytic process has been proposed.

2. Experimental details

2.1. Materials

Zinc acetate dihydrate, nickel acetate tetrahydrate, and sodium hydroxide (NaOH) received from Aladdin Co. Ltd. Triethanolamine (EDTA), benzoquinone (BQ), and isopropyl alcohol (IPA) were obtained from Sinopharm Group Chemical Reagent Co., Ltd. A Ti_3C_2 MXene was purchased from Foshan XinXi Technology Co., Ltd. All reagents used were utilized without extra processing.

2.2. Materials synthesis

First, 2 g of Ti_3C_2 MXene (10 mg/mL) was diluted in a volume of 20 mL of water. Next, 30 mL of zinc acetate dihydrate (2 M) was put into a previous solution. Subsequently, 3 mL of ammonia solution (25%) and 4 g of NaOH (5%) were gradually introduced into the solution dropwise while stirring continuously for a duration of 15 minutes.. When the temperature reached 60 ℃, 1.5 mL of a 0.2M solution of nickel acetate was added to the solution while stirring continuously for 5 minutes.. The combined solution was thereafter put into a 100 mL autoclave and maintained at a temperature of 160 ℃ for a duration of 15 hours. The precipitate was formed through the process of centrifugation and subsequent washing with water multiple times. It was then dried at a temperature of 80 ℃.. The products that were obtained were identified as Ni-ZnO NR/Ti_3C_2. For comparison, pure ZnO NR (without Ti_3C_2 addition and nickel acetate) and Ni-ZnO NR (without Ti_3C_2 addition) were also produced through the same method.

2.3. Characterization

The morphology of the materials was analyzed using scanning electron microscopy (SEM, Hitachi S4800) and transmission electron microscopy (TEM, JEOL JEM-2100F). The crystal structures were analyzed using X-ray diffraction (XRD) with a D5000 instrument. The elemental composition was examined using an X-ray photoelectron spectrometer (XPS), specifically the Thermo Scientific K-Alpha 1063 model. The optical characteristics were examined by UV-Vis diffuse reflection spectroscopy (UV-2550, Shimadzu) and photoluminescence spectroscopy (PL, IHR550, Horiba).

2.4. Photocatalytic performance

The photocatalytic activity was assessed by conducting a removal process of methyl orange (MO). To achieve this objective, a solution containing 25 mL of MO (10 mg/L) and 25 mg of the sample was agitated for 30 minutes in the absence of light. Subsequently, the solution underwent irradiation using a 300 W xenon lamp that imitated solar light. Aliquots of 3 mL were then subjected to observations on a UV-visible spectrometer at 15-minute intervals. The samples' efficiency was assessed using the formula $[(C_0-C_e)/C_0]\times 100$, where C0 represents the initial concentration of MO and Ce represents the concentration after the reaction.

The radical trapping studies were conducted in a comparable manner, with the exception that 2 mL of each scavenger (0.02 M) were utilized, including EDTA (quencher of h^+), BQ (quencher of $\bullet O_2^-$), and IPA (quencher of $\bullet$OH), were added to the Ni-ZnO NR/Ti_3C_2 solution, which was then exposed to illumination for 60 min.

3. Results and discussion

The physical characteristics and arrangement of components on the surface within the Ni-ZnO NR/Ti_3C_2 composite were evaluated utilizing SEM and EDS. As shown in Fig. 1a, ZnO possessed the rod-like structure, in which the lengths and diameters of rods were ~2 μm and 500 nm, respectively. Ti_3C_2 MXene particles had a typical flaky shape and were attached intimately to ZnO nanorods (shown with the arrow in Fig. 1a). The EDS element mapping analysis (Fig. 1b) proved the existence of Zn, O, Ni, Ti, and C elements in the composite.

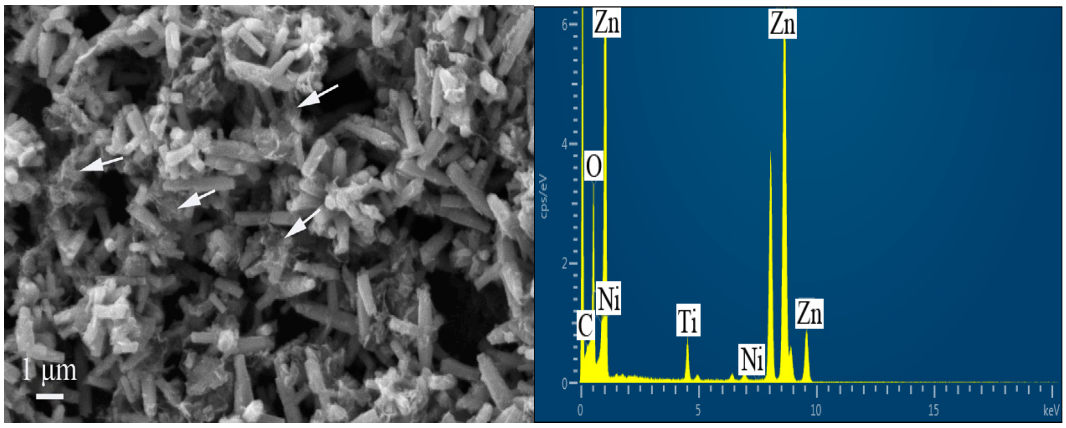

(a) (b)

Fig. 1. (a) SEM, (b) EDS of Ni-ZnO NR/Ti_3C_2.

The TEM images of Ni-ZnO NR/Ti_3C_2 are depicted in Fig. 2. According to Fig. 2a, ZnO possessed a well-defined rod-like structure, which was in agreement with the above SEM observation. Ti_3C_2 MXene exhibited an ultrathin sheet structure with slight wrinkles on the edge. Furthermore, ZnO nanorods were deposited on the MXene nanosheets, which resulted in the formation of a ZnO/Ti_3C_2 MXene heterojunction. In the HRTEM image (Fig. 2b), a dashed line denotes the presence of a distinctly discernible heterojunction between ZnO and Ti_3C_2 MXene. The inter-planar spacings within ZnO and Ti_3C_2 components were measured to be 0.27 nm and 0.23 nm, corresponding to the ZnO (100) and Ti_3C_2 (103) planes, respectively [14,15]. The investigation of element mapping in EDS (Figs. 2c-h) demonstrated the evenly dispersed Ni, Zn, O, Ti, and C elements, further confirming the successful formation of ZnO nanorods and Ti_3C_2 MXene.

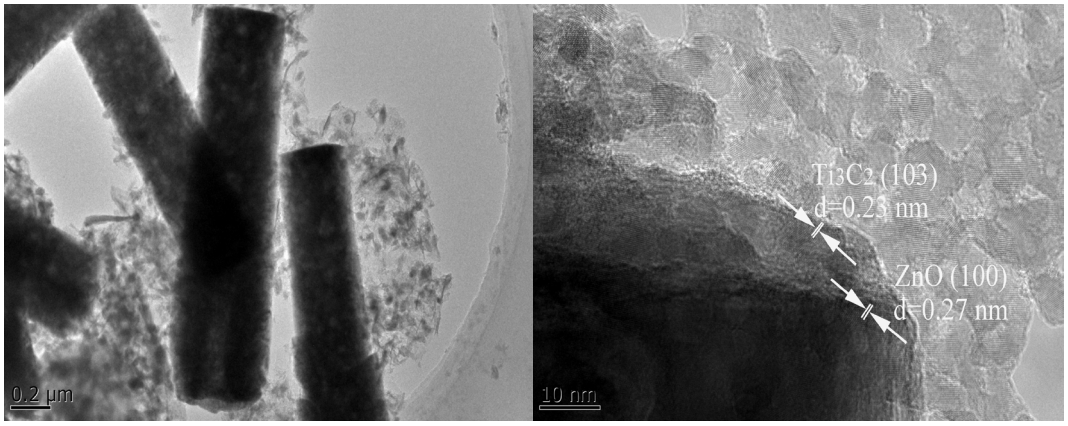

(a) (b)

Fig. 2.1 (a)TEM images, (b) HRTEM lattice image,

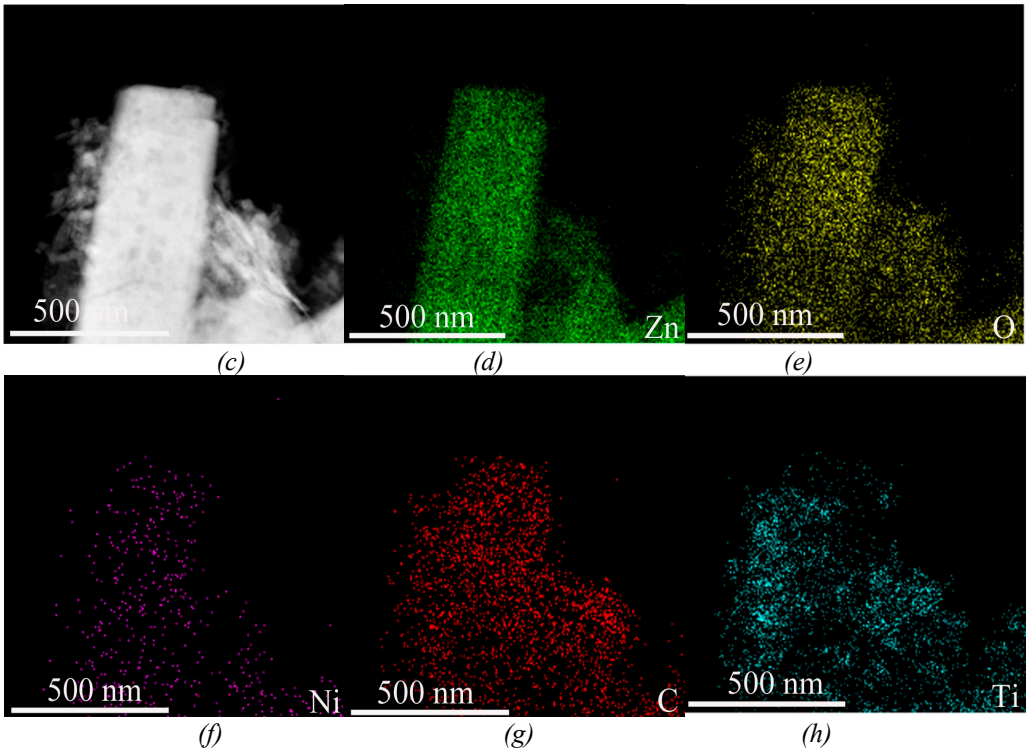

(c) (d) (e)

(f) (g) (h)

Fig. 2.2 (c) STEM, (d-h) EDS elemental mapping images of Ni-ZnO NR/Ti_3C_2.

For investigating the crystal structures and phases within the samples, the XRD study was conducted, and the corresponding XRD profiles are shown in Fig. 3. The distinctive peaks of ZnO NRs were located at 31.7°, 34.4°, 36.2°, 47.5°, 56.5°, 62.9°, 66.3°, 68.0° and 69.0°, equivalent to the (100), (002), (101), (102), (110), (103), (200), (112) and (201) planes of a hexagonal ZnO wurtzite phase (JCPDS 01-079-2205) [16]. As for the Ni-ZnO NR, the respective peak locations were slightly shifted toward the higher values, indicating the incorporation of Ni^{2+} into the ZnO lattice [17]. Furthermore, the Ni-ZnO NR/Ti_3C_2 displayed a characteristic diffraction peak of Ti_3C_2 MXene [18], which revealed the successful preparation of Ni-ZnO/Ti_3C_2 nanocomposites.

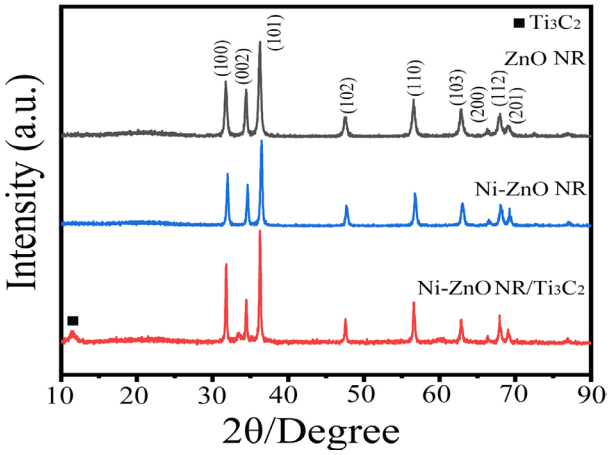

Fig. 3. XRD pattern of the samples.

Fig. 4 shows the optical absorption properties of the samples. The pure ZnO NRs, Ni-ZnO NRs, and Ni-ZnO NR/Ti_3C_2 demonstrated absorption at around 395 nm, 408 nm, and 420 nm, respectively. This indicated that pure ZnO NRs possessed the pronounced UV light absorption, whereas Ni-ZnO NR and Ni-ZnO NR/Ti_3C_2 exhibited a redshift and the obvious enhancement of the visible-light absorption [18]. As illustrated in Fig. 4b, the estimated bandgap values for ZnO, Ni-ZnO and Ni-ZnO/Ti_3C_2 were 3.20, 3.16 and 3.10 eV, correspondingly, which showed that Ni-ZnO NR/Ti_3C_2 composite had the narrowest bandgap among all samples. The results revealed that Ni doping of ZnO NRs and the fine interface in the Ni-ZnO NR/Ti_3C_2d composite provided the synergistic effect, which was beneficial for the photocatalytic performance [19].

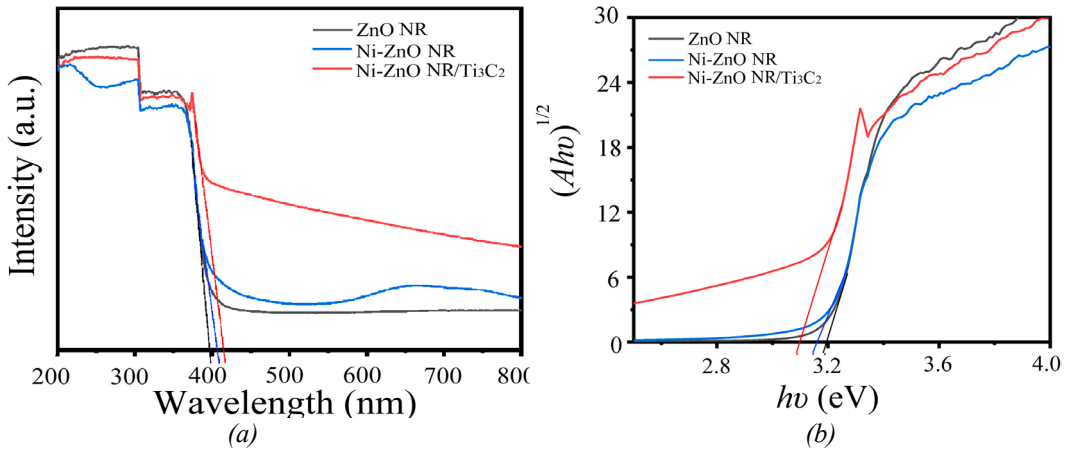

Fig. 4. (a)UV-Vis absorption spectra, (b) plots of (Ahν)1/2 versys photon energy (hν) of samples.

The PL spectroscopy study was carried out to explore the effectiveness of carrier separation at the specific wavelength of 370 nm that causes excitation. Demonstrated in Fig. 5, Ni-ZnO NR/Ti_3C_2 had the lowest PL peak compared with ZnO NRs and Ni-ZnO NRs, indicating the lowest recombination of excited electrons and holes via the Schottky junction and thus the longest carrier lifetime [20]. This further proved the synergistic effect between Ni-doped ZnO and Ti_3C_2.

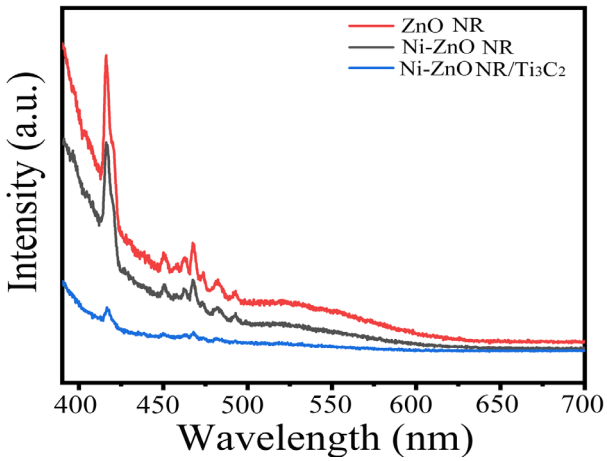

Fig. 5. PL spectra of the samples.

Fig. 6 depicts the chemical composition of the Ni-ZnO NR/Ti_3C_2, determined by means of an X-ray photoelectron spectrometer (XPS). According to Fig. 6a, there were Zn 2p, O 1s, Ni 2p, Ti 2p, and C 1s peaks observed in the survey XPS spectrum of Ni-ZnO NR/Ti_3C_2, and the atomic percentages of Zn, O, Ni, Ti and C elements in the Ni-ZnO NR/Ti_3C_2 were 33.1%, 41.0%, 3.3%, 2.5%, 5.4% and 14.7%, respectively, indicating that Ni-ZnO NR/Ti_3C_2 were successfully prepared. The Zn 2p XPS spectrum displayed two peaks at 1021.2 and 1044.4 eV (Fig. 6b) [21]. The O 1s XPS spectrum was resolved into three peaks, among which those at 530.0 and 531.6 eV were associated with Zn-O and O-H bonds (Fig. 6c). The presence of the C-Ti-(OH) bond caused the peak at 532.4 eV. The data provided evidence for the presence of ZnO in the composites and the formation of covalent bonds between ZnO and Ti_3C_2 MXene [22]. The Ni 2p XPS spectrum displayed four peaks at 855.3, 861.3, 872.6, and 879.3 eV. The located characteristics at 872.6 and 855.3 eV was credited to the Ni 2p1/2 and Ni 2p3/2 states, and those at 861.3 and 879.3 eV were the respective satellite peaks, which proved that Ni^{2+} was successfully introduced into ZnO (Fig. 6d) [23]. The Ti 2p XPS spectrum was deconvoluted into three peaks: There are two distinct energy peaks in the X-ray photoelectron spectroscopy (XPS) spectrum of Mxene. One peak is centered at 454.2 eV, which corresponds to the Ti-C bond, while the second peak is centered at 458.1 eV, showing the presence of Ti-Ti bonds. These peaks provide information about the primary chemical state of titanium in Mxene. The third signal was detected at 463.6 eV, corresponding to Ti-O bonds. This suggests a close electrical connection between Ti_3C_2 MXene and ZnO. (Fig. 6e) [24]. Fig. 4f displays the C 1s point at 284.4 eV, which corresponds to the presence of C-C bonds. The presence of C-O-C bonds was identified by a peak at 288.7 eV.[25]. Therefore, the XPS and XRD results strongly evidenced the formation of ZnO/Ti_3C_2 MXene composite and Ni doping of the ZnO lattice.

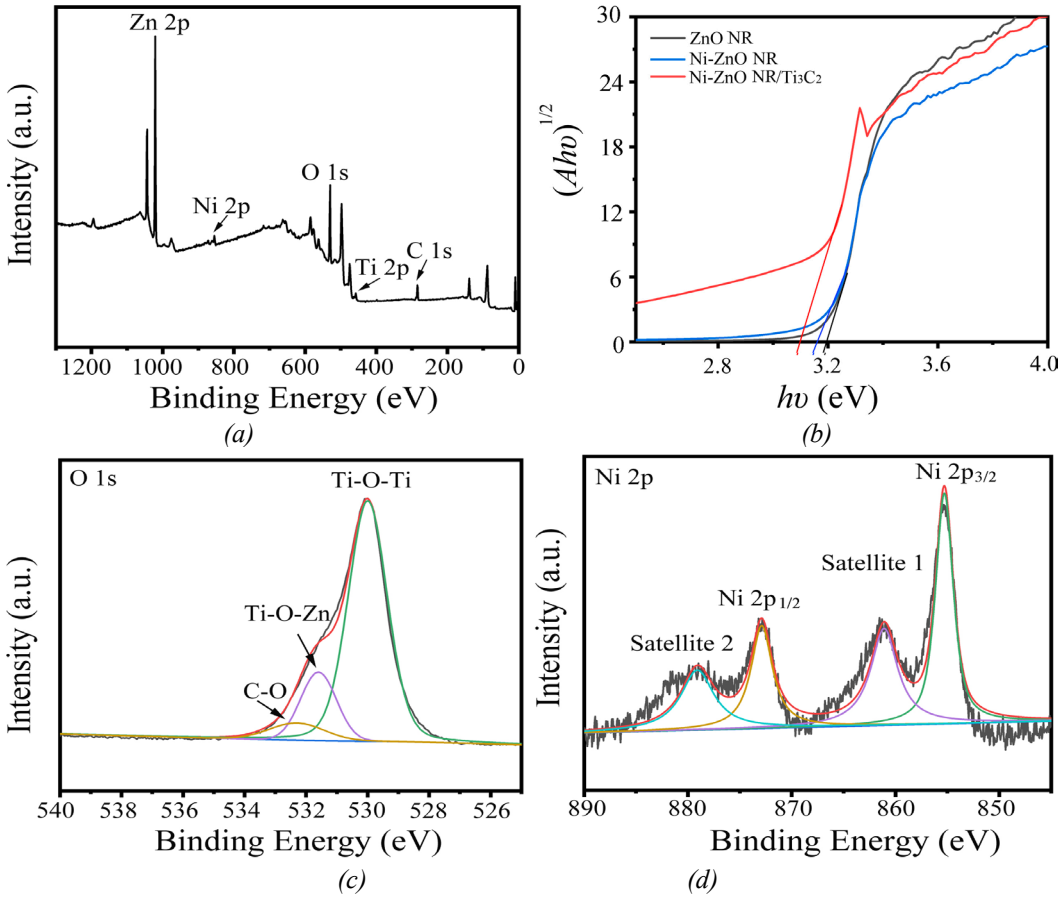

Fig. 6.1. XPS curves of the samples, (a) the survey spectra, (b) The Zn core level (2p) spectra, (c) The O core level (1s) spectra , (d) The Ni core level (2p) spectra, (d) The Ti core level (2p) spectra

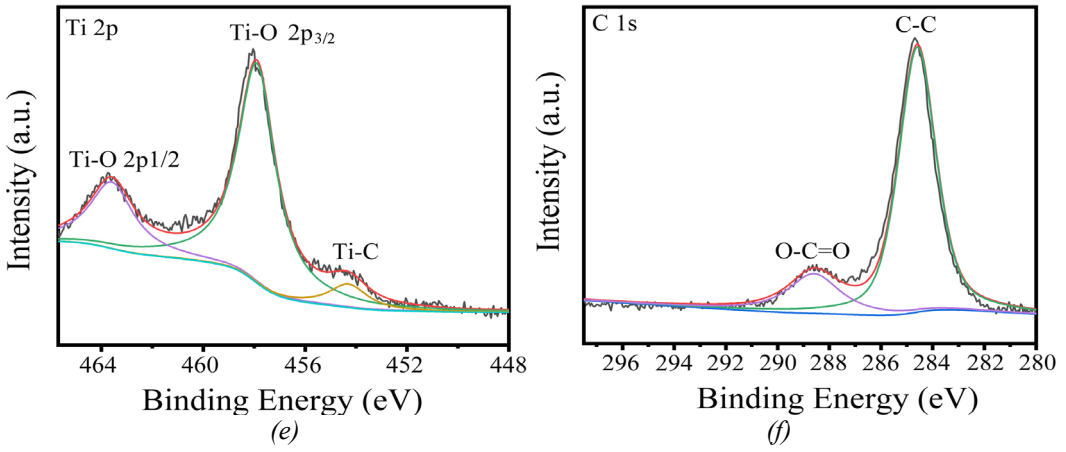

Fig. 6.2. XPS curves of the samples, e) f) The C core level (1 s) spectra.

Fig. 7 Shows the photocatalytic degradation curves and corresponding kinetic properties of MO when exposed to simulated solar light irradiation.. According to the data, only 16.0% and 9.7% of MO were degraded by pure ZnO NRs and Ti_3C_2 MXene, respectively, indicating unsatisfactory photocatalytic efficiency (Fig. 7a). In turn, the MO degradation rates increased to 69.1% for Ni-ZnO NRs, meaning that Ni-doped ZnO possessed the narrower bandgap and could fully benefit from solar light irradiation. As for the Ni-ZnO NR/Ti_3C_2 composite, it had the highest MO removal rate (88.2%). Demonstrated in Fig. 7b, the calculated rate constants of Ti_3C_2, ZnO

NRs and Ni-ZnO NRs were respectively 0.00141, 0.00212 and 0.0163 min^{-1}. The highest reaction rate constant (0.02824 min^{-1}) was achieved in Ni-ZnO NR/Ti_3C_2 composite, being 20.0, 13.3 and 1.7 times those of ZnO NRs, Ti_3C_2 MXene and Ni-ZnO NRs, respectively. The enhanced dye degradation might be ascribed to the fast charge transfer in the Schottky junction formed in ZnO NR/Ti_3C_2 MXene composite, as well as the pronounced visible light absorption in Ni-doped ZnO.

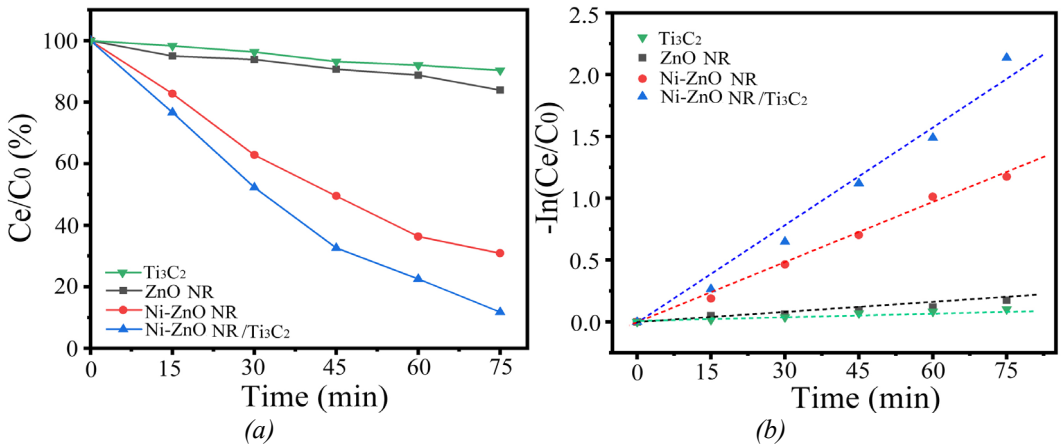

Fig. 7. (a) Degradation efficiency, (b) Kinetic curves.

The main active species were identified by several scavengers, as shown in Fig. 8a. It could be seen that no obvious effect was observed from the BQ scavenger, while there was a remarkable drop by IPA and EDTA scavengers, indicating that •OH and h^+ radicals played the main role in the photocatalytic reaction.

According on the above discussion, the potential mechanism of Ni-ZnO NR/Ti_3C_2 composite was proposed, as shown in Fig. 8b. Once Ni entered the ZnO lattice, a new doping level was formed between the valence band and the conduction band. When the Ni-ZnO NR/Ti_3C_2 composite and when ZnO was subjected to visible light, the electrons from its valence band were stimulated to a higher energy level. and left holes, thus forming the electron-hole pairs [26]. Because the Fermi level of Ti_3C_2 MXene was lower than the doping level conduction band, the photoinduced electrons would rapidly transfer to the layered Ti_3C_2 MXene, resulting in a Schottky barrier formation at the ZnO/Ti_3C_2 interface without returning back to ZnO [27]. Superoxide anion radicals (•O_2^-) could be created due to these produced electrons attacking O_2 molecules. Meanwhile, holes in the valence band (VB) interacted with H_2O, promoting the emergence of •OH radicals [28]. Both were strong oxidants for decomposing dye molecules. The complete process of photodegradation can be succinctly stated as follows:

$$\text{Ni-ZnO NR/}Ti_3C_2 + h\nu(\text{solar-simulated light}) \rightarrow \text{Ni-ZnO NR/}Ti_3C_2\ (h^+(VB) + e^-(CB))$$

$$\text{Ni-ZnO NR/}Ti_3C_2\ (e^-(CB)) \rightarrow \text{MXene}\ (e^-(CB))$$

$$\text{MXene}\ (e^-(CB)) + H^+ + O_2 \rightarrow H_2O_2$$

$$H_2O_2 + e^- + h\nu \rightarrow \bullet OH + OH^-$$
$$VB\ (h^+) + H_2O \rightarrow H^+ + \bullet OH$$

$$\bullet OH + \text{Pollutant} \rightarrow H_2O + CO_2$$

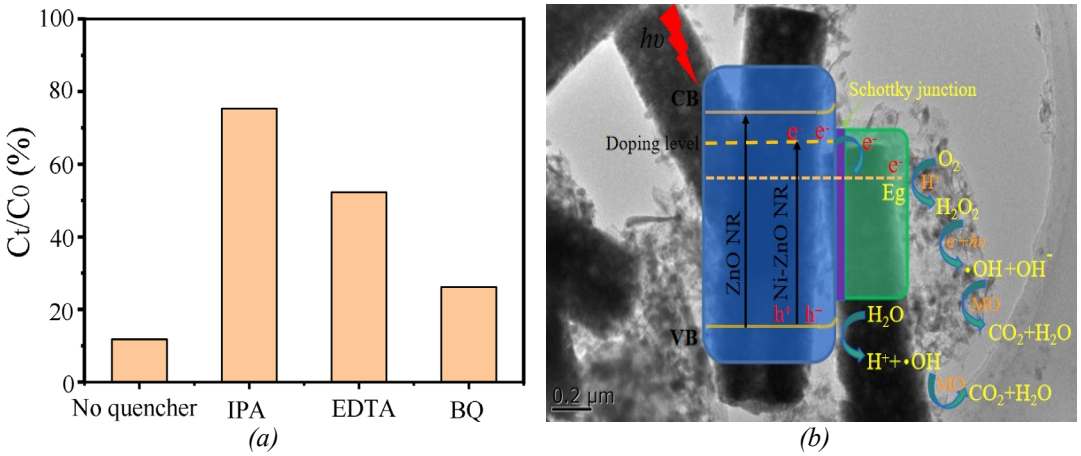

Fig. 8. Schematic photocatalytic reaction mechanism for Ni-ZnO NR/Ti_3C_2 composite.

4. Conclusions

A Ni-ZnO NR/Ti_3C_2, a catalyst was synthesized using a hydrothermal technique., exhibiting the prominent photocatalytic activity on MO. The enhancement of the photocatalytic efficiency of the synthesized nanocomposites might be attributed to the following reasons. First, the one-dimensional ZnO nanorods were conducive to the fast electron transfer and provided the effective catalytic activity. Second, the Schottky barrier between ZnO and Ti_3C_2 MXene prohibited the electron-hole pair recombination and prevented electrons from returning back to ZnO. Third, Ni-doped ZnO narrowed the bandgap of ZnO and promoted the visible light absorption. Therefore, this study provides a new route to develop Ti_3C_2 MXene materials with the outstanding photocatalytic activity.

Acknowledgments

This work was supported by the National Natural Science Foundation of Hunan Province, China (No. 2024JJ7305, 2024JJ7312, 2024JJ7248).

References

[1] Z. G. Li, B. Zeng. Dig. J. Nanomater. Bios. 16(2), 725 (2021).
[2] F.Y. Li, H.L. Xu, F. Feng, et al., Journal of Hunan University of Arts and Science (Science and Technology), 35(4), 62 (2023).
[3] A. Goktas, S. Modanl, A. Tumbul, et al., J Alloy. Compd. 893, 162334 (2022); https://doi.org/10.1016/j.jallcom.2021.162334
[4]M. Khadidja, J. Fan, S. Li, et al., Colloid. Surface. A 628(5), 127230 (2021); https://doi.org/10.1016/j.colsurfa.2021.127230
[5] W. Zhou, B. Yu, J. Zhu, et al., Appl. Surf. Sci. 590(15), 153095 (2022); https://doi.org/10.1016/j.apsusc.2022.153095
[6]M.T. Liu, J.Y. Li, R.M. Bian, et al., J. Alloy compd. 905, 164025 (2022); https://doi.org/10.1016/j.jallcom.2022.164025
[7]V.T. Quyen, L.T. Ha, D.M. Thanh, et al., Environ. Technol. Inno. 21, 101286 (2021).
[8]W. Yu, J. Zhang, T. Peng, Appl. Catal. B Environ. 181, 220 (2016); https://doi.org/10.1016/j.apcatb.2015.07.031
[9]M. A. Qamar, M. Javed , S. Shahid, et al., Mater. Res. Bull. 147, 111630 (2022);

https://doi.org/10.1016/j.materresbull.2021.111630
[10]R. Behnood, G. Sodeifian. J Environ. Chem. Eng. 8, 103821 (2020);
https://doi.org/10.1016/j.jece.2020.103821
[11]A. Bahadur, S. Iqbal, H.O. Alsaab, et al., RSC Adv. 11, 36518 (2021);
https://doi.org/10.1039/D0RA09390D
[12]L.M. Jose, S.A. Thomas, A. Aravind, et al., Inorg. Chem. Commun. 147, 110208 (2023);
https://doi.org/10.1016/j.inoche.2022.110208
[13]M.R. Al-Mamun, M.Z. Rokon, M. Abdur Rahim, et al., Heliyon 9, e16506 (2023);
https://doi.org/10.1016/j.heliyon.2023.e16506
[14]E. Rdewi, K. Abbas, A. AbdulkadhimAl-Ghaban, Mater. Today. 60, 1702 (2022);
https://doi.org/10.1016/j.matpr.2021.12.229
[15]B. Zeng, X.T. Ning, L.F. Li. J. Alloy compd. 963, 171309 (2023);
https://doi.org/10.1016/j.jallcom.2023.171309
[16]A. Das, P. M. Kumar, M. Bhagavathiachari, et al., Appl. Surf. Sci. 534, 147321 (2020);
https://doi.org/10.1016/j.apsusc.2020.147321
[17]P. Gnanamozhi, V. Renganathan, S.M. Chen. et al., Ceram. Inter. 46, 18322 (2020);
https://doi.org/10.1016/j.ceramint.2020.05.054
[18]J. Ran, G. Gao, F.T. Li, et al., Nat. Commun. 8, 13907 (2017);
https://doi.org/10.1038/ncomms13907
[19]B. Zeng, X.T. Ning, L.F. Li, et al., Dig. J. Nanomater. Bios. 17(3), 881 (2022);
[20]L. Zhang, P Ma, L Dai, et al., Chem. Eng. J. Adv. 10(15), 100285 (2022);
https://doi.org/10.1016/j.ceja.2022.100285
[21]X. Liu, H. Zhang, Y. Song, et al., Actuat. B. Chem. 367, 132025 (2022);
https://doi.org/10.1016/j.snb.2022.132025
[22]J. Ran, G. Gao, F.T. Li, et al., Nat. Commun. 8, 13907 (2017);
https://doi.org/10.1038/ncomms13907
[23]J. Xu, M. Li, L. Yang, et al., Chem. Eng. J. 394, 125050 (2020);
https://doi.org/10.1016/j.cej.2020.125050
[24]Y. Qian, H. Wei, J. Dong, et al., Ceram. Inter. 43(14), 10757 (2017);
https://doi.org/10.1016/j.ceramint.2017.05.082
[25] A. Sreedhar, J.S. Noh., J. Electroanal. Chem. 883(15), 115044 (2021);
https://doi.org/10.1016/j.jelechem.2021.115044
[26]N. Elumalai, S. Prabhu, M. Selvaraj, et al., Chemosphere. 291, 132782 (2022);
https://doi.org/10.1016/j.chemosphere.2021.132782
[27]W. Song, Q. Liu, J. Chen, et al., Small, 17, 2100439 (2021);
https://doi.org/10.1002/smll.202100439
[28] I. Alsafari. Ceram. Inter. 48(8), 10960 (2022);
https://doi.org/10.1016/j.ceramint.2021.12.315